Available online at www.sciencedirect.com
ScienceDirect
Journal of Power Sources 175 (2008) 166–174
JOURNAL OF POWER SOURCES
www.elsevier.com/locate/jpowsour

Platinum nanoparticles supported on activated carbon fiber as catalyst for methanol oxidation

Hui Xing Huang [a], Shui Xia Chen [a,b,*], Chan'e Yuan [a]

[a] PCFM Lab, OFCM Institute, School of Chemistry and Chemical Engineering, Sun Yat-Sen University, Guangzhou 510275, PR China
[b] Materials Science Institute, Sun Yat-Sen University, Guangzhou 510275, PR China

Received 16 June 2007; received in revised form 29 August 2007; accepted 30 August 2007
Available online 7 September 2007

Abstract

Activated carbon fiber (ACF) with high specific surface area has been used as support in the preparation of Pt nanoparticles electrocatalyst (Pt/ACF) for direct alcohol fuel cells. It is found that the Pt nanoparticles on ACF are highly and homogeneously dispersed with a narrow size distribution in the range of 1.5–3.5 nm with an average size of 2.4 nm. In comparison with the commercial E-TEK Pt/C catalyst, the Pt/ACF catalyst exhibits much higher catalytic activity for methanol, ethanol and isopropanol oxidation, which are about 2.4 times as high as that of the former. The Pt/ACF catalyst is observed to be significantly more stable during the constant current density polarization and continuous cyclic voltammetry in comparison with Pt/C catalyst. Both the uniform dispersion of Pt nanoparticles and strong interactions between Pt nanoparticles and ACF are of benefit to achieve the performance improvement of Pt/ACF catalyst.

Keywords: Activated carbon fiber support; Platinum; Electrocatalyst; Methanol oxidation; Fuel cell

1. Introduction

Direct alcohol fuel cells (DAFCs) have attracted considerable interest primarily due to their promising applications as power sources for electric vehicles and portable electronics [1]. The performance of DAFCs greatly depends on catalytic activity and durability of the catalyst. It has been reported that the natures of the carbon supports determine the dispersion and stability of the metal crystallites, the electronic properties of the metal, including metal–support interactions and mass transfer resistances of the catalyst layer [2–4]. Therefore, special attention has been given to alternative carbon materials as catalyst supports for DAFCs, including carbon nanotubes [5,6], mesocarbon microbeads [7], ordered mesoporous carbons [8,9], carbon nanofibers [10,11], and other structured carbons [12–14].

Carbon blacks have been successfully used as supports in commercial catalysts for fuel cells, however, self-agglomeration of the carbon particles limits the approach of the fuel and oxidant to the active sites, and therefore the electrocatalyst efficiency of the fuel-cell electrode will be reduced.

It is well known that fibers offer flexibility which does not apply to the usual powdery or granular materials. Fibrous catalytic packs offer the advantages of an immobile catalyst and a short diffusion distance. Another advantage of fibrous catalysts is their low resistance to flow of liquid and gases through a bundle of fibers. Thus, they can be used as an attractive alternative in fuel cell.

With plentiful micropores and a huge surface area thus resulting in high adsorption capacity, activated carbon fiber (ACF), described as a novel kind of porous material, plentiful functional groups on whose surface have strong reactivity. In addition, plentiful functional groups on the surface of activated carbon fiber also have strong reactivity. In addition, ACF has such a reduction property that it can reduce Pt(IV) into a lower valence ion and Pd(II), Ag(I), Au(III) ions into metallic elements [15–20] which leads to a promising application of being used in the preparation of catalysts.

In this paper, the uniform dispersion of Pt nanoparticles supported on activated carbon fiber with a high specific surface area was prepared. The morphology of the Pt catalyst was

* Corresponding author at: PCFM Lab, OFCM Institute, School of Chemistry and Chemical Engineering, Sun Yat-Sen University, Guangzhou 510275, PR China. Tel.: +86 20 84112093; fax: +86 20 84034027.
E-mail address: cescsx@mail.sysu.edu.cn (S.X. Chen).

0378-7753/$ – see front matter © 2007 Elsevier B.V. All rights reserved.
doi:10.1016/j.jpowsour.2007.08.107

characterized by transmission electron microscopy (TEM). The electrocatalytic properties of the Pt/ACF catalyst for alcohols oxidation were evaluated by cyclic voltammetry and chronoamperometry. The electrochemical stability of the Pt/ACF catalyst was studied by chronopotentiometry and continuous cyclic voltammetry.

2. Experimental

2.1. Materials

All the chemical reagents employed in this study were of analytical grade. Chloroplatinic acid was purchased from ShenYang Jin Ke Chemical Factory, China. Vulcan XC-72 carbon black was purchased from Cabot Inc., 20 wt.% Pt supported on Vulcan carbon black (Pt/C) catalyst from E-TEK Inc. and Nafion 5 wt.% solution from Dupont.

2.2. Preparation of ACF and Pt/ACF catalyst

Viscose fiber was carbonized at 850 °C in N_2 atmosphere and activated using steam as an activation agent at the same temperature for 60 min. Viscose-based activated carbon fiber thus obtained had diameters of about 10 μm. Pore structure of ACF is summarized in Table 1.

The catalyst was prepared according to the following procedures: 80 mg of ACF was first suspended in ultrapure water; then 5.4 mL of 0.0193 mol dm^{-3} chloroplatinic acid mixed with ethylene glycol was added into the above suspension solution, 2 mol dm^{-3} NaOH was gradually added to the suspended mixture until the pH of the mixed solution reached 13 and the mixture was refluxed at 130 °C for 3 h. The resulting solid was washed with distilled water until Cl^- anion was not detected by $AgNO_3$ solution and then dried in vacuum at 80 °C. Pt supported on ACF catalyst with a metal loading of 20 wt.%, denoted as Pt/ACF, was obtained. The ratio of Pt to ACF was controlled by the stoichiometric calculation, and Pt content on Pt/ACF catalyst was also confirmed by atomic absorption spectroscopy (AAS) measurement. The AAS analysis of filtrate showed that platinum was completely deposited on the ACF.

2.3. Structural characterization and electrochemical evaluations

Specific surface areas and pore volumes of carbons were measured on a volumetric adsorption apparatus from Micromeritics (Norcross, GA, USA) at 77.4 K using nitrogen gas as the adsorbate in the relative pressure range from 10^{-6} to 0.995. The sample was degassed at 200 °C in vacuum for 8 h before measurement.

Transmission electron microscope (TEM) was performed on a JEOL JEM-2010HR operating at 200 kV. Samples were prepared by ultrasonically suspending the catalysts powder in ethanol. A drop of the slurry was then deposited onto a clean holey carbon–copper grid and the ethanol was allowed to evaporate. More than 200 particles were measured to get integrated information about size distribution and average size of every Pt-based catalyst sample.

X-ray diffraction (XRD) scans were obtained on a Rigaku D/MAX 2200VPC X-ray diffractometer using Cu Kα radiation (λ = 0.154056 nm). The tube voltage was maintained at 40 kV and tube current at 48 mA. The 2θ angles ranging from 20° to 90° were explored at a scan rate of 5° min^{-1}. The Pt(2 2 0) peak (60° to 75°) was scanned at 1° min^{-1} with a resolution of 0.02° in order to obtain the size information of Pt crystallites by Scherrer formula.

All electrochemical measurements were performed in a three-electrode electrochemical cell on an IM6ex electrochemical workstation (Zahner-Electrik, Germany) at room temperature. For the preparation of working electrodes, 5 mg of Pt/ACF catalyst or 5 mg of Pt/C catalyst (20 wt.%, from E-TEK), 50 μL of Nafion solution (5 wt.%, Dopont), and 4 mL of isopropyl aqueous solution ($V_{alcohol}$:V_{water} = 1:3) were mixed ultrasonically. The well-mixed electrocatalyst ink (20 μL) was deposited onto the surface of a freshly polished glassy carbon disk (GC, 3 mm in diameter and 0.07065 cm^2) and dried at 80 °C for 30 min. Based on the volume of electrocatalyst ink deposited onto the carbon electrode, the Pt loadings on the Pt/C and Pt/ACF electrodes were calculated to be 0.07 mg cm^{-2}. A Pt foil and a saturated calomel electrode (SCE) were used as the counter and the reference electrodes, respectively. N_2 gas was purged for 20 min before the experiment started.

3. Results and discussion

3.1. Pore structure of activated carbon fiber

Specific surface area of sample was determined by Brunauer–Emmet–Teller (BET) method applied in a relative pressure range from 0.05 to 0.35 and micropore volume as well as micropore area by t-plot method. The total volume (V_{total}) was calculated by converting the adsorption amount of N_2 at a relative pressure of 0.95 into its liquid volume. Pore structure parameters of ACF and Vulcan XC-72 are listed in Table 1.

The results indicated that the ACF employed in this study had a specific surface area of 1338 m^2 g^{-1} – which was five times larger than that of Vulcan XC-72 (224 m^2 g^{-1}) – and a micropore area of 873 m^2 g^{-1}, which meant it was significantly microporous. The analysis based on the nitrogen adsorption isotherms also indicated that the average micropore diameter based on

Table 1
Pore structure parameters of ACF and Vulcan XC-72

Samples	S_{BET} (m^2 g^{-1})	S_{micro} (m^2 g^{-1})	S_{meso} (m^2 g^{-1})	V_{total} (cm^3 g^{-1})	V_{micro} (cm^3 g^{-1})	V_{meso} (cm^3 g^{-1})	D_{total} (nm)
ACF	1338	873	465	0.648	0.402	0.246	2.66
Vulcan XC-72	224	91	133	0.305	0.042	0.263	7.72

Dubinin–Astakhov method is about 0.59 nm, and diameters of the micropores mostly distribute in a range from 0.5 to 1.2 nm. Interestingly, the sample got an average pore diameter (4V/S) of 2.6 nm for total pores (micropore and mesopore), which would be close to the size of Pt particles supported on ACF. It is found that higher surface area will be advantageous to both a better dispersion of Pt particles and higher loading of Pt catalysts. Furthermore, a higher surface area increases the three-phase interface for electrode, and that will be convenient for mass transportation of reactant and products [21].

3.2. Particle size and distribution of Pt on carbon supports

The X-ray diffraction patterns of the catalysts and carbon supports are shown in Fig. 1. The broad peaks at $2\theta = 24^\circ$ and about 44° correspond to the diffraction of graphite crystallite of Vulcan XC-72 and the ACF supports, while the peaks at 39.6°, 46.3°, 67.8° and 81.6° are due to Pt(1 1 1), Pt(2 0 0), Pt(2 2 0) and Pt(3 1 1) face-centered cubic phases, respectively. The Pt(2 0 0) peak was scanned at $1^\circ\ \mathrm{min}^{-1}$ ranging from 60° to 75°, which is shown in the inset of Fig. 1. In order to avoid the disturbance caused by the diffraction of graphite crystallite, the average crystallite sizes of Pt supported on Vulcan XC-72 and the ACF were calculated based on the broadening of the Pt(2 0 0) peak from Scherrer equation:

$$d = \frac{0.9\lambda}{B\cos\theta} \quad (1)$$

where d is the average particle sizes (nm), λ the wave-length of X-ray radiation (0.154056 nm) and B is the width (in radians) of the diffraction peak at half height. The results indicated that Pt supported on ACF excelled that on Vulcan XC-72 in crystallite size, which of 2.9 and 2.1 nm diameter, respectively belonged to Pt/C and Pt/ACF. However, XRD measurements cannot supply exact information of crystallite size when it is less than 3.0 nm, for this reason, the figures obtained by the above equation will be slightly smaller than true ones.

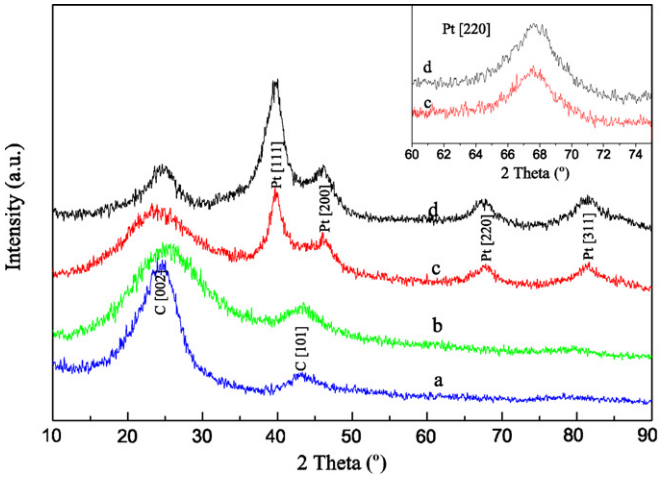

Fig. 1. The X-ray diffraction patterns of Pt/ACF and Pt/C. Inset: detailed Pt(2 2 0) peaks. (a) Vulcan XC-72 (b) ACF (c) Pt/ACF and (d) Pt/C.

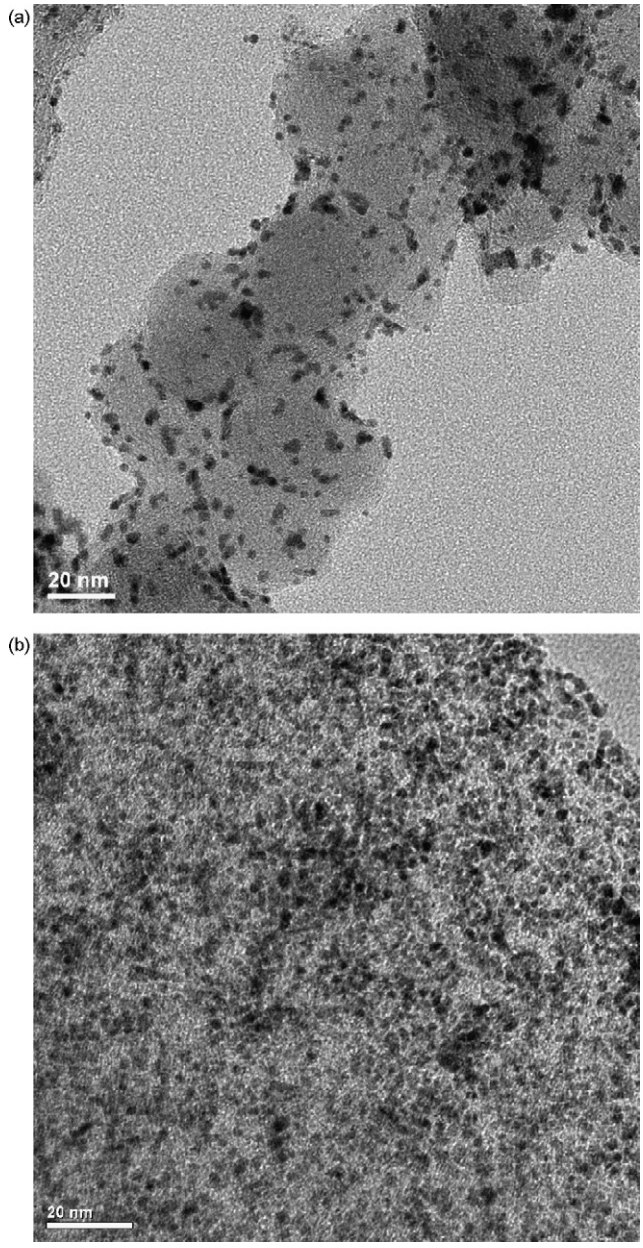

Fig. 2. TEM images of Pt/C (a) and Pt/ACF (b) catalysts.

Fig. 2 shows TEM images of Pt/ACF and Pt/C catalysts. The size distribution of Pt particles on the catalysts was also obtained by directly measuring over 200 particles from TEM micrographs, and the corresponding histograms of which are shown in Fig. 3. These results showed that the spherical Pt particles deposited on ACF were fairly uniform and well distributed and the particle size distribution, ranging from 1.5 to 3.5 nm, was rather narrow. On the contrary, the Pt particles were apparently agglomerated and thus have a bad dispersion on Vulcan XC-72, leading to a much broader particle size range from 1.0 to 9.0 nm. The mean size was estimated to be 2.4 nm for Pt/ACF and 2.9 nm for Pt/C, which was in good agreement with the results from XRD.

As it is well known, activated carbon fiber has abundant open micropores on its surface, by which certain amount of water

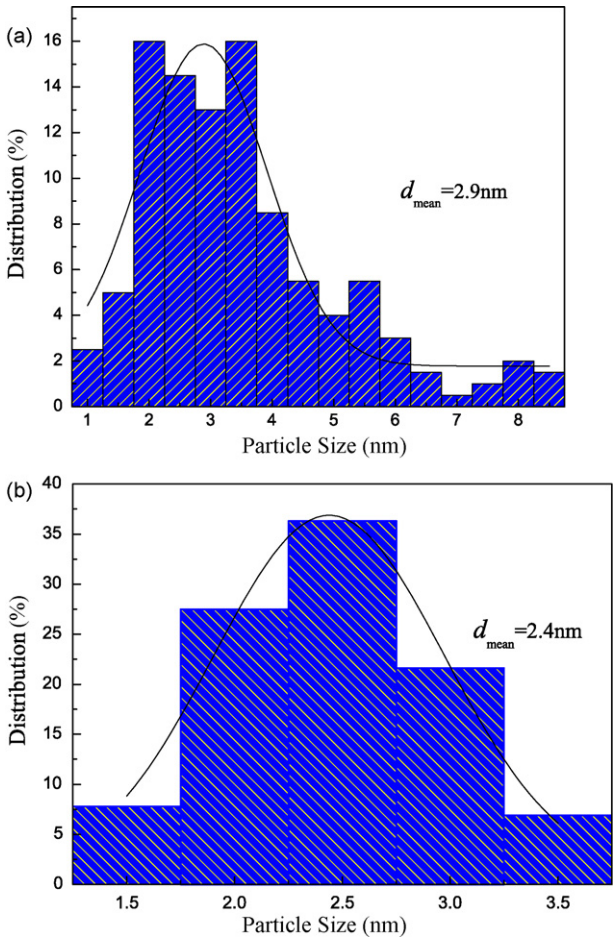

Fig. 3. Distributions of diameters of Pt nanoparticles on Pt/C (a) and Pt/ACF (b) catalysts.

can be absorbed during the preparation process. In addition, the $PtCl_6^{2-}$ ions in ethylene glycol solvent are more easily to dissolve in water and then strongly adsorb on the walls of the micropores. With the pH and temperature of the solution adjusted to proper values, most of Pt precursors captured by open micropores were reduced in situ, thereby preventing Pt particles from coalescence into larger particles. Vulcan XC-72 where the micropores in the core were concealed by the graphitic shell, deposition of Pt particles had to occur on the graphitic shell. As a result, the reduction in the available surface area of Vulcan XC-72 for deposition had led to larger particles being formed [22].

Fig. 4 shows the high-resolution TEM (HRTEM) images of Pt/C and Pt/ACF catalysts. The image (see Fig. 4a) revealed that the Pt crystallites dispersed on ACF had relatively good crystallographic orientation, suggesting the establishment of a strong metal–support interaction. It might be due to the strong interactions between Pt particles and ACF, which are caused by the abundant functional groups such as carboxyl, hydroxyl and carbonyl groups on the surface of supports. Meanwhile, surface basic sites of ACF are associated with π-electron rich regions within the basal planes, which is also responsible for the strong adsorption of Pt. In contrast, Pt particles supported on Vulcan XC-72 were found to adopt a more dense globular morphology

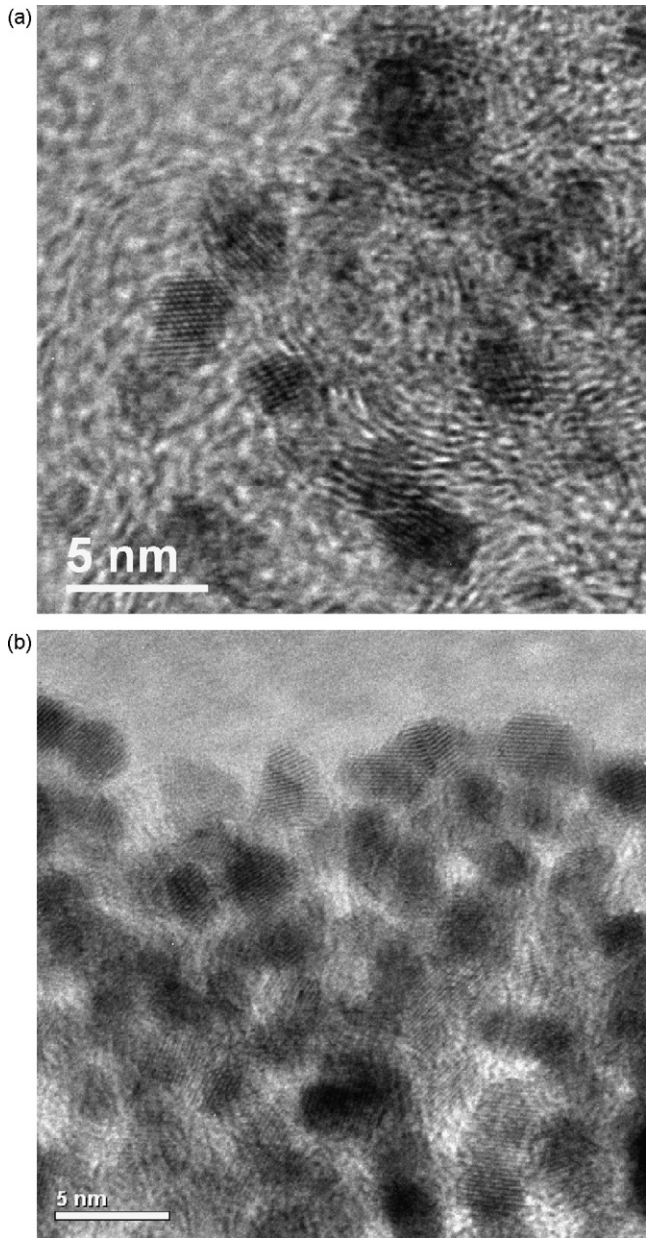

Fig. 4. HRTEM images of Pt/C (a) and Pt/ACF (b) catalysts.

(see Fig. 4b), suggesting that in this case there was a relatively weak interaction with the metal and support [10].

3.3. Electrocatalytic properties of Pt/ACF catalyst for alcohol

The cyclic voltammograms of Pt/ACF and Pt/C catalysts in 1 mol dm^{-3} CH_3OH and 0.5 mol dm^{-3} H_2SO_4 solutions are shown in Fig. 5. The anodic current density of Pt/ACF catalyst in the forward scan increased with the scan potential, and reached its maximum peak current density, 24.9 mA cm^{-2} at 0.65 V, which was significantly higher than that of Pt/C catalysts (10.2 mA cm^{-2}), and indicated that the Pt/ACF catalyst had excellent catalytic activity on methanol electrooxidation. The onset potential of methanol oxidation on Pt/ACF catalyst

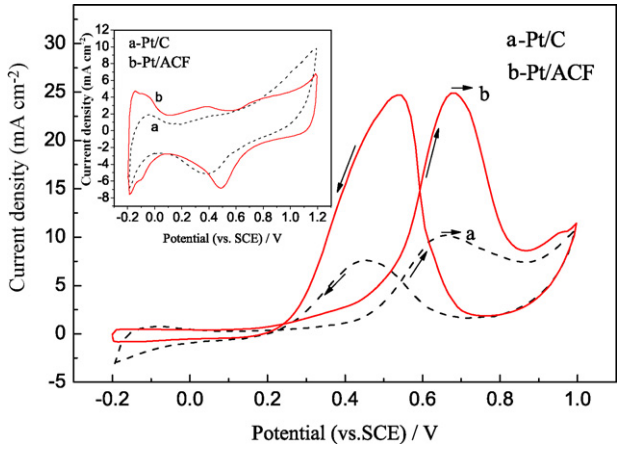

Fig. 5. Cyclic voltammograms of methanol oxidation on Pt/ACF and Pt/C in 1 mol dm^{-3} CH_3OH/0.5 mol dm^{-3} H_2SO_4 solution at 20 mV s^{-1}, room temperature. Inset: cyclic voltammograms of Pt/ACF and Pt/C in 0.5 mol dm^{-3} H_2SO_4 solution at 50 mV s^{-1}.

occurred at 0.1 V, which showed a significant negative shift of about 150 mV compared to Pt/C catalysts. The better performance of methanol electrooxidation on Pt/ACF catalyst could be attributed to a suitable and uniform particle size of well-dispersed Pt particles supported on the ACF surface.

The cyclic voltammograms of Pt/ACF and Pt/C catalysts in 0.5 mol dm^{-3} H_2SO_4 solutions are shown in the inset of Fig. 5. For Pt/ACF catalysts, well-defined hydrogen adsorption–desorption peaks with a much larger area were observed in the potential region from −0.2 to 0.1 V, demonstrating a larger electrochemical active surface area of the catalyst. Also, the large surface area was owing to the presence of narrow size and uniform distribution of the Pt particles on ACF as displayed in the TEM micrograph before. Electrochemical active surface (EAS) of Pt can be calculated from the following formula [23]:

$$\mathrm{EAS} = \frac{Q_H}{0.21 \times [\mathrm{Pt}]} \quad (2)$$

where [Pt] represents the platinum loading (mg cm^{-2}) in the electrode, Q_H the amount of charge exchanged during the electroadsorption of hydrogen atoms on Pt (mC cm^{-2}) and a correlation value of 0.21 (mC cm^{-2}) the charge required to oxidize a monolayer of H_2 on poly-crystalline Pt electrodes. The electrochemical active areas of platinum on Pt/ACF and Pt/C catalyst calculated by the above Eq. (2) were 65.3 and 23.8 m^2 g^{-1}, respectively. We believe that a numbers of reasons could cause a large difference in the electrochemical active surface area of Pt/ACF and Pt/Vulcan though they had similar particle sizes and Pt loadings. First, fibers catalytic packs offer the advantages of a short diffusion distance and a low resistance to flow of liquid and gases through a bundle of fibers, which provide them a very excellent adsorption performance than that of a powdered or granulated bed. Activated carbon fibers with plenty of active carbon–oxygen groups have also been found to be extremely hydrophilic. Therefore, fluid transport through the hydrophilic fiber is faster than through Vulcan XC-72. Second, because Pt particles are enclosed and sheltered by the carbon black agglomeration, the approach of protons to the active sites will be limited. The self-agglomeration and uneven distribution of Pt particles as shown in Fig. 2a will also reduce the electrocatalyst efficiency of the fuel-cell electrode. In contrast, the even distribution of Pt particles will enhance the effective contacting with protons. Thus it is reasonable that the catalyst support on the ACF has a higher electrochemical active surface area than that prepared with Vulcan XC-72.

Table 2
Comparison of the peak current density and onset potentials of alcohols oxidation on Pt/C and Pt/ACF electrodes

	Methanol	Ethanol	Isopropanol
Pt/C			
j_p (mA cm^{-2})	10.3	6.4	2.9
E_s (V)	0.25	0.52	0.04
Pt/ACF			
j_p (mA cm^{-2})	24.9	11.6	5.8
E_s (V)	0.10	0.30	−0.04

The oxidation of methanol, ethanol and isopropanol on Pt/C and Pt/ACF electrodes were examined. Table 2 summarizes the corresponding values of the onset potentials (E_s) and peak current densities (j_p) for alcohols oxidation on Pt/C and Pt/ACF electrodes in 0.5 mol dm^{-3} H_2SO_4/1 mol dm^{-3} alcohols aqueous solutions at 20 mV s^{-1}, respectively. The peak current densities for alcohols oxidation on Pt/ACF electrode were almost twice as that on Pt/C electrode; furthermore, the onset potentials for Pt/ACF electrocatalyst were also significant negative shift compared with Pt/C electrocatalyst. All in all, Pt/ACF electrocatalyst showed the better performance for alcohols oxidation than that of Pt/C.

In order to make a comparison between the activities of Pt/ACF and Pt/C catalysts for methanol electrooxidation, the steady-state current densities at a constant potential were used. Fig. 6 shows the change of polarization currents with time of methanol electrooxidation on Pt/ACF and Pt/C catalysts at 0.4 V versus SCE. The initial high current corresponded mainly to double-layer charging. The Pt/ACF and Pt/C catalysts presented

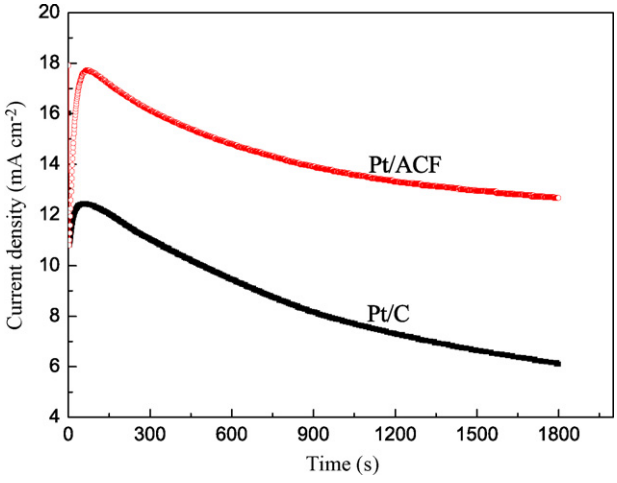

Fig. 6. Chronoamperometric curves (at 0.4 V vs. SCE) of methanol oxidation on Pt/ACF and Pt/C in 1 mol dm^{-3} CH_3OH/0.5 mol dm^{-3} H_2SO_4 solutions.

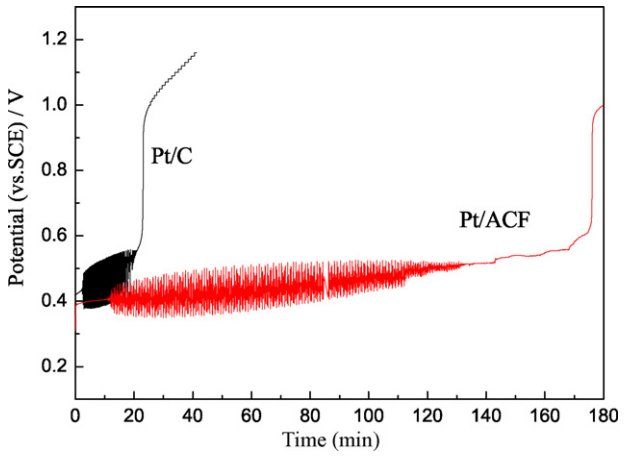

Fig. 7. Potential/time plots of Pt/ACF and Pt/C in 1 mol dm^{-3} CH_3OH/0.5 mol dm^{-3} H_2SO_4 solutions at 6 mA cm^{-2}.

continuous decay in activity with time, which would due to the intermediate products of methanol oxidation such as CO adsorbed on the Pt particles, which would inhibit electrooxidation reaction of methanol. After a polarization of 1800 s, Pt/ACF and Pt/C catalysts reached their steady-state current of 12.6 and 6.1 mA cm^{-2}, respectively. In addition, the current density of Pt/ACF catalysts behaved with a more gently decreasing trend, which was possibly owing to the larger active area of Pt particles supported on ACF. All the facts indicated that Pt/ACF catalyst displayed better performances for methanol electrooxidation than Pt/C catalyst [24].

As shown in Fig. 7, the respective chronopotentiometric curves for methanol oxidation on Pt/ACF and Pt/C catalysts at 6 mA cm^{-2} were dramatically different. The potentials of Pt/ACF and Pt/C catalysts increased gradually with the lasting of polarization time and finally shifted to a higher value for oxygen evolution rather than methanol oxidation, indicating the poisoning of the catalyst [25]. From the results, it can be seen that the Pt/ACF catalyst can be operated at a lower overpotential and last a longer time to be poisoned at the same current density. The better stability of the Pt/ACF catalyst towards methanol oxidation might be attributable to the uniform Pt nanoparticles on ACF, which can supply more active sites for methanol oxidation, and also the attainment of a preferred crystallographic orientation by the Pt nanoparticles as a result of the interaction with the ACF.

It is well known that change in the morphology of the catalyst layer from the initial state will result in a loss of electrochemical activity. This loss of activity in the Pt/C catalysts due to the agglomeration of platinum particles is considered to be a major cause of the decrease in cell performance [26,27]. The durability performance for Pt/ACF and Pt/C catalysts was directly evaluated by the change in the active surface area of catalyst during the continuous cycles test.

Fig. 8 shows a subset of the CVs obtained at room temperature from the Pt/ACF and Pt/C catalysts during a total of 1800 cycles. The Pt active surface area was determined by integrating the hydrogen desorption peak of the cyclic voltammogram. The data indicated that the Pt/C underwent significant changes, whereas

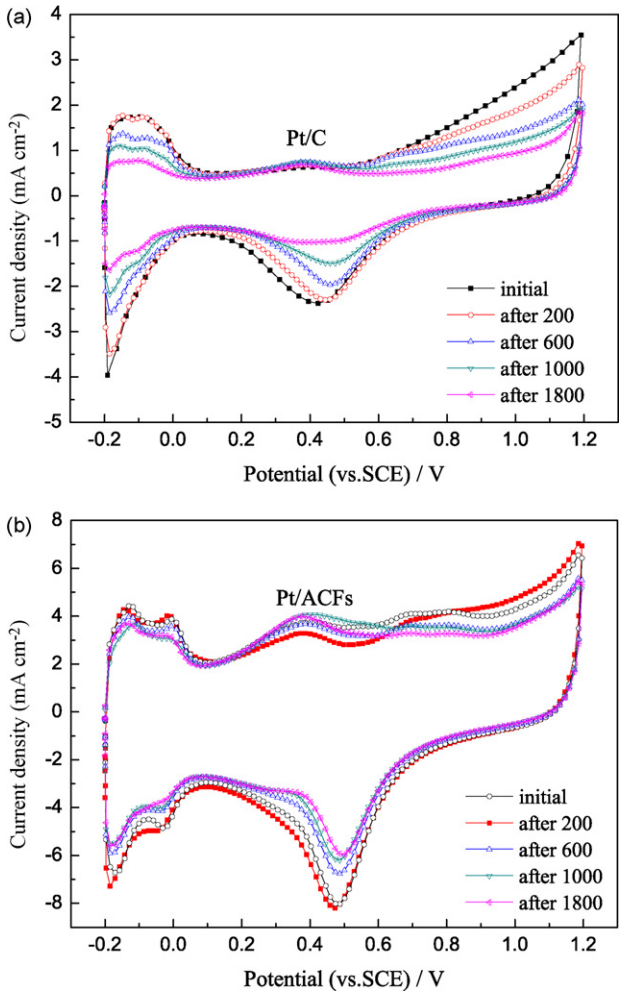

Fig. 8. Cyclic voltammograms of Pt/C (a) and Pt/ACF (b) in 0.5 mol dm^{-3} H_2SO_4 at 50 mV s^{-1} (in the potential range −0.2 to 1.0 V vs. SCE cycling at 100 mV s^{-1} in 1 mol dm^{-3} CH_3OH/0.5 mol dm^{-3} H_2SO_4 solution on Pt/C and Pt/ACF after 0, 200, 600, 1000 and 1800 cycles).

the Pt/ACF was much more stable. The initial Pt surface areas of Pt/C and Pt/ACF catalysts before the continuous cycles test were 24.9 and 63.8 m^2 g^{-1}, respectively. While almost 37.4% of Pt surface area was lost for Pt/C catalyst over 1000 cycles, only 14.6% loss was observed for Pt/ACF catalyst. Additionally, almost 55% of Pt surface area was lost for Pt/C catalyst over 1800 cycles, however, after 1000 cycles, with an unconspicuous decreasing rate for Pt/ACF catalyst, which remained only 14.2% of loss in Pt surface area even after 1800 cycles. The results indicated that ACF could potentially provide much higher durability than Vulcan XC-72.

Fig. 9 shows TEM images of Pt/ACF and Pt/C catalysts before and after stability test. It was obvious that the platinum particles basically maintained their high dispersion on the ACF after 1800 cycles; though some of them grew slightly larger and got closer together during the stability test. It is well known that high surface area of carbon support would help to increase the platinum dispersion and effectively prevent extensive growth and aggregation of platinum particles. On the other hand, it is possible that the slit shaped micropores densely opening toward the outer surface of the fiber can also anchor platinum nanoparticles and

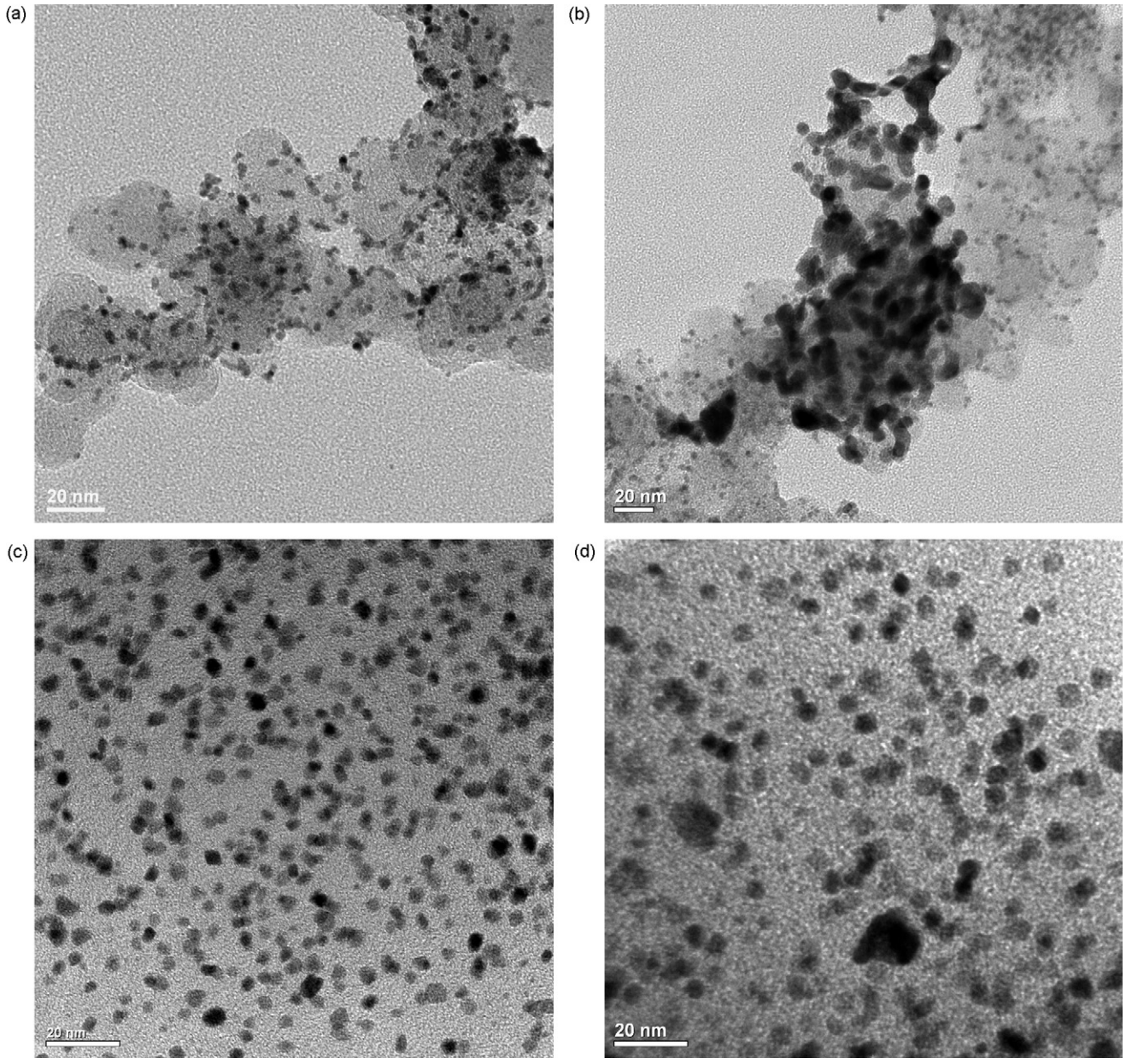

Fig. 9. TEM images of Pt/ACF and Pt/C catalysts before and after stability test. (a and c) Pt/C and Pt/ACF before stability test; (b and d) Pt/C and Pt/ACF after stability test for 1800 cycles.

alleviate the Pt migration. In contrast, for Pt/C, platinum particles significant sintering occurred after 1800 cycles. Fig. 9b shows evidence for necking between platinum particles on Vulcan XC-72. The mean size increased from 2.9 to 7.3 nm for Pt/C after stability test. This was in agreement with the trend observed for Pt surface area change. It was due to the self-aggregation of carbon black particles, which could facilitate the migration, and aggregation platinum particles to form larger particles, which also was the reason that Pt/C underwent significant decrease in electrochemical active surface areas.

Fig. 10 summarizes the changes in the retention ratio of electrochemically active surface areas of Pt/ACF and Pt/C catalysts. The retention value of active surface area of Pt/ACF catalyst was gradually decreased with repetitious cycles to show the minimum value of 85.4% at around 1000 cycles and its value tended to keep constant afterwards, whereas the value for the Pt/C catalyst continued to drastically decrease down to 45% at 1800 cycles. It would reveal that the micropore structure on the surface of ACF hold the Pt nanoparticles on the edge of the micropore, and prevent them from aggregating to bigger particles, thus resist the loss of the effective surface area of Pt catalyst [28].

Obviously, long-term cycle stability of catalyst for methanol oxidation is another important parameter in practical application of DAFCs. Anodic peak current density of Pt/ACF and Pt/C catalysts during a total of 1800 cycles are shown in Fig. 11. For each catalyst, the peak current density obtained from the forward CV scan rise at first until it attained the maximum value and

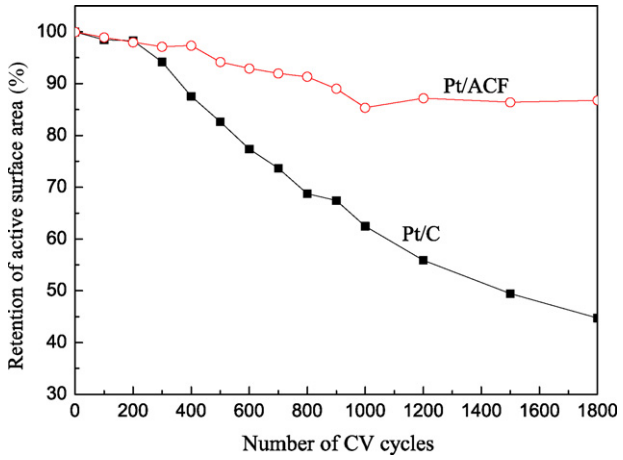

Fig. 10. Change in retention ratio of electrochemical active surface areas of Pt/C and Pt/ACF with different cycle numbers in 1 mol dm^{-3} CH_3OH/0.5 mol dm^{-3} H_2SO_4 solutions at 100 mV s^{-1}, room temperature.

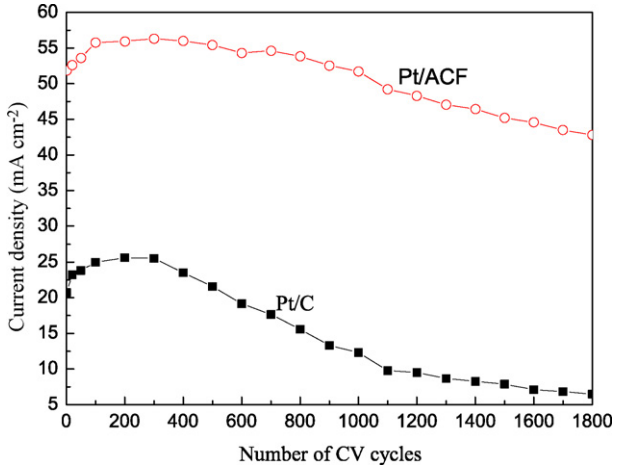

Fig. 11. Anodic peak current density of Pt/C and Pt/ACF with different cycle numbers in 1 mol dm^{-3} CH_3OH/0.5 mol dm^{-3} H_2SO_4 solutions at 100 mV s^{-1}, room temperature.

afterwards displayed a downward trend with the successive CV scans. For Pt/ACF catalyst, its peak current density approached a maximum at 56.32 mA cm^{-2} at the 300th scan, after which the value slid down gently, with an acceptable decrease of 24.1%, eventually to 42.78 mA cm^{-2} at the 1800th scan. On the other hand, for the Pt/C catalyst, the peak current density reached its maximum at 25.64 mA cm^{-2} at the 200th scan, and then drastically decreased down to 6.49 mA cm^{-2} at the 1800th scan, with a striking decrease of 74.7%. By all appearances, Pt/ACF catalyst performed excellent stability and outstanding catalytic activity, was a welcome contrast to commercial E-TEK Pt/C catalyst.

4. Conclusions

By using the reactive activity of activated carbon fiber, fine and homogeneous Pt particles can be successfully supported on ACF, and the Pt/ACF catalyst for fuel cell can be easily obtained by this liquid phase chemical reduction method. All the experimental results reveal that Pt/ACF shows both higher catalytic activity and electrochemical stability in alcohols oxidation. The anodic current densities of alcohols oxidation on Pt/ACF are twice as high as those on commercially available E-TEK Pt/C catalyst with same Pt loading (20 wt.%). The fibrous support, with abundant functional groups and plentiful micropore on the surface, offers the advantages of a short diffusion distance and a strong interaction between Pt particles and carbon support, which efficiently resist the agglomeration of Pt particles and the loss in active surface area of the catalyst during continuous cycling. This might be the reason why the Pt/ACF catalyst performs significantly better electrochemical stability than commercial Pt/C catalyst.

Acknowledgment

The authors gratefully acknowledge the support by the National Natural Science Foundation of China (no. 50373053).

References

[1] C. Lamy, A. Lima, V. LeRhun, F. Delime, C. Coutanceau, J.M. Léger, J. Power Sources 105 (2002) 283–296.
[2] T. Matsui, T. Okanishi, K. Fujiwara, K. Tsutsui, R. Kikuchi, T. Takeguchi, K. Eguchi, Sci. Technol. Adv. Mater. 7 (2006) 524–530.
[3] G. Selvarani, A.K. Sahu, N.A. Choudhury, P. Sridhar, S. Pitchumani, A.K. Shukla, Electrochim. Acta 52 (2007) 4871–4877.
[4] H.S. Liu, C.J. Song, L. Zhang, J.J. Zhang, H.J. Wang, D.P. Wilkinson, J. Power Sources 155 (2006) 95–110.
[5] G.L. Che, B.B. Lakshmi, E.R. Fisher, C.R. Martin, Nature 393 (1998) 346–349.
[6] W.Z. Li, C.H. Liang, W.J. Zhou, J.S. Qiu, H.Q. Li, G.Q. Sun, Q. Xin, Carbon 42 (2004) 436–439.
[7] Y.C. Liu, X.P. Qiu, Y.Q. Huang, W.T. Zhu, J. Power Sources 111 (2002) 160–164.
[8] S.H. Joo, S.J. Choi, I. Oh, J. Kwak, Z. Liu, O. Terasaki, R. Ryoo, Nature 412 (2001) 169–172.
[9] S.H. Joo, C. Pak, D.J. You, S.A. Lee, H.I. Lee, J.M. Kim, H. Chang, D. Seung, Electrochim. Acta 52 (2006) 1618–1626.
[10] C.A. Bessel, K. Laubernds, N.M. Rodriguez, R. Baker, K. Terry, J. Phys. Chem. B 105 (2001) 1115–1118.
[11] F. Yuan, H. Ryu, Nanotechnology 15 (2004) S596–S602.
[12] J.L. Figueiredo, M.F.R. Pereira, P. Serp, P. Kalck, P.V. Samant, J.B. Fernandes, Carbon 44 (2006) 2516–2522.
[13] S. Han, Y. Yun, K. Park, Y. Sung, T. Hyeon, Adv. Mater. 15 (2003) 1922–1925.
[14] G.S. Chai, S.B. Yoon, J.H. Kim, J.S. Yu, Chem. Commun. 23 (2004) 2766–2767.
[15] S.X. Chen, J.R. Liu, H.M. Zeng, J. Mater. Sci. 40 (2005) 6223–6231.
[16] H.T. Zheng, Y.L. Li, S.X. Chen, P.K. Shen, J. Power Sources 161 (2006) 371–375.
[17] S.X. Chen, R.M. Xu, X.P. Zhang, H.M. Zeng, J. React. Polym. 11 (2002) 108–112.
[18] S.X. Chen, H.M. Zeng, Carbon 41 (2003) 1265–1271.
[19] S.X. Chen, R.M. Xu, H.X. Huang, H.M. Zeng, Chin. J. Ion Exch. Adsorp. 22 (2006) 9–15.
[20] R.M. Xu, S.X. Chen, H.X. Huang, Chin. J. Funct. Mater. 37 (2006) 604–606.
[21] F.Y. Xie, Z.Q. Tian, H. Meng, P.K. Shen, J. Power Sources 141 (2005) 211–215.
[22] J.H. Zeng, F.B. Su, J.Y. Lee, W.J. Zhou, X.S. Zhao, Carbon 44 (2006) 1713–1717.
[23] A. Pozio, M. De Francesco, A. Cemmi, F. Cardellini, L. Giorgi, J. Power Sources 105 (2002) 13–19.
[24] R. Hughes, Deactivation of Catalysts, Academic Press, 1984, pp. 6.

[25] J. Lee, C. Eickes, M. Eiswirth, G. Ertl, Electrochim. Acta 47 (2002) 2297–2301.
[26] S.Y. Ahn, S.J. Shin, H.Y. Ha, S.A. Hong, Y.C. Lee, T.W. Lim, I.H. Oh, J. Power Sources 106 (2002) 295–303.
[27] M.K. Debe, A.K. Schmoeckel, G.D. Vernstrom, R. Atanasoski, J. Power Sources 161 (2006) 1002–1011.
[28] X.S. Zhao, G.Q. Sun, W.M. Chen, S.H. Tang, Q. Xin, S.H. Yang, B.L. Yi, Chin. J. Catal. 26 (2005) 383–388.